

RESEARCH ARTICLE

10.1002/2014JD021470

Key Points:

- The North American heat wave was a key factor in the 2012 Greenland melting
- Transport of warm air and water vapor to Greenland was via an Atmospheric River
- Many factors in 1889 the last melting episode were very similar to those in 2012

Supporting Information:

- Readme
- Supplemental Material

Correspondence to:

W. Neff,
William.Neff@noaa.gov

Citation:

Neff, W., G. P. Compo, F. M. Ralph, and M. D. Shupe (2014), Continental heat anomalies and the extreme melting of the Greenland ice surface in 2012 and 1889, *J. Geophys. Res. Atmos.*, *119*, 6520–6536, doi:10.1002/2014JD021470.

Received 15 JAN 2014

Accepted 18 APR 2014

Accepted article online 24 APR 2014

Published online 11 JUN 2014

Continental heat anomalies and the extreme melting of the Greenland ice surface in 2012 and 1889

William Neff^{1,2}, Gilbert P. Compo^{1,2}, F. Martin Ralph³, and Matthew D. Shupe^{1,2}

¹NOAA Earth System Research Laboratory, Physical Sciences Division, Boulder, Colorado, USA, ²Cooperative Institute for Research in the Environmental Sciences (CIRES), University of Colorado, Boulder, Colorado, USA, ³Scripps Institution of Oceanography, La Jolla, California, USA

Abstract Recent decades have seen increased melting of the Greenland ice sheet. On 11 July 2012, nearly the entire surface of the ice sheet melted; such rare events last occurred in 1889 and, prior to that, during the Medieval Climate Anomaly. Studies of the 2012 event associated the presence of a thin, warm elevated liquid cloud layer with surface temperatures rising above the melting point at Summit Station, some 3212 m above sea level. Here we explore other potential factors in July 2012 associated with this unusual melting. These include (1) warm air originating from a record North American heat wave, (2) transitions in the Arctic Oscillation, (3) transport of water vapor via an Atmospheric River over the Atlantic to Greenland, and (4) the presence of warm ocean waters south of Greenland. For the 1889 episode, the Twentieth Century Reanalysis and historical records showed similar factors at work. However, markers of biomass burning were evident in ice cores from 1889 which may reflect another possible factor in these rare events. We suggest that extreme Greenland summer melt episodes, such as those recorded recently and in the late Holocene, could have involved a similar combination of slow climate processes, including prolonged North American droughts/heat waves and North Atlantic warm oceanic temperature anomalies, together with fast processes, such as excursions of the Arctic Oscillation, and transport of warm, humid air in Atmospheric Rivers to Greenland. It is the fast processes that underlie the rarity of such events and influence their predictability.

1. Introduction

An increase in the melt rate of the Greenland ice sheet, particularly at lower elevations, has been reported in recent years [Fettweis *et al.*, 2013; Tedesco *et al.*, 2013] and attributed in part to an increased frequency of anticyclones positioned over Greenland producing increased southerly flow west of Greenland. However, melting at the highest elevations on the ice sheet surface has been extremely rare compared to lower elevations: an analysis of the Greenland Ice Sheet Project 2 ice core near Summit Station (72°34' N, 38°29' W, 3212 m ASL), on the very top of the ice sheet, revealed approximately centennial time-scale surface melt episodes during the recent Holocene from 750 A.D. to 1250 A.D. with very thin melt layers in the ice core indicative of temperatures exceeding freezing [Meese *et al.*, 1994]. These coincided with the extended Medieval Climate Anomaly (MCA) and a period of mega-droughts over regions of North America [Cook *et al.*, 2010]. Such melting episodes are also evident earlier over the last 10,000 years with a highly variable frequency of occurrence [Alley and Anandakrishnan, 1995]. After a long hiatus, a melt event again occurred in 1889 at Summit [Meese *et al.*, 1994]. This event was also confirmed by radar mapping of internal layers in the ice [Kanagaratnam *et al.*, 2001]. The next, and most recent, Summit melt episode occurred in July 2012. By 12 July, nearly the entire surface of Greenland showed evidence of melting in satellite retrievals [Nghiem *et al.*, 2012] while under the influence of warm air advection [Fettweis *et al.*, 2013] and the radiative effects of warm, low-level liquid layer clouds [Bennartz *et al.*, 2013]. These liquid-water clouds were thick enough, together with warmer air aloft, to cause enhanced downwelling infrared heating of the surface but thin enough to allow penetration of solar radiation to the surface at Summit Station where the 2 m temperature rose above the melting point on 11 July. The detailed analysis in Bennartz *et al.* [2013] took advantage of measurements of cloud, radiation, microphysics, and surface energy balance that were in place as part of a multi-year study at Summit Station [Shupe *et al.*, 2013].

NOAA tower temperature measurements (2 m) at Summit Station during the summer of 2012 recorded three extended warm periods with a modest maximum on 15 June (−1.8°C), warming above the melting point on 11 July (+0.8°C), and warming to near-melting temperatures on 29 July (−0.4°C). By way of comparison, the previous two summers recorded unusually warm 2 m temperatures at Summit: −1.9°C on 13 June 2011 and

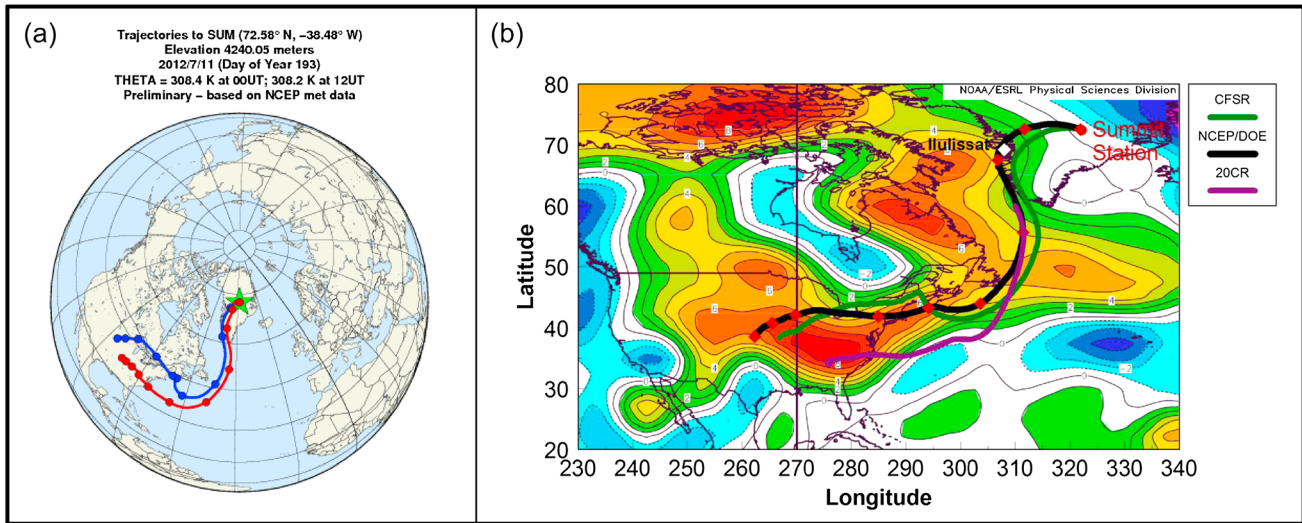


Figure 1. Trajectory analysis for the 11 July Greenland melt episode. (a) Isentropic back trajectories from 1 km above Summit Station for air parcels arriving on 11 July using the NOAA/GMD trajectory tool. Isentropic paths, marked in daily increments, from the central US for the 00 Z (UT, blue) and 12 Z (UT, red) 11 July back trajectories starting on 1 July are shown. Table 1 lists the daily temperatures and pressure heights along the isentropes. (b) Temperature anomaly (925 hPa) over the US for 1 July from the NCEP/DOE reanalysis. Back-trajectories (700 hPa) are shown: Heavy Black (NCEP/DOE), dark Green (CFSR) and purple (20CR) are averages for the four 6 h trajectories. The 20CR trajectory is not well behaved over the topography of Greenland so that trajectory starts at 60°N, 310E at 700 hPa on a point along the NCEP/DOE reanalysis. The only weather station with daily data recorded for 1889, Ilulissat, is indicated by the white diamond on the plot and lies along the trajectory to Summit Station.

−2.0°C on 18 June 2010. The second two warm periods in 2012 at Summit Station correspond to a nearly geographically complete melt of the ice sheet surface (98.6%) by 12 July and a substantial melt (79.2%) on 29 July, respectively, as documented by satellite imaging [Nghiem *et al.*, 2012]. Of interest here are the other factors and precursors coming together on 11 and 29 July at Summit that may not have been present in other events that “only” reached temperatures close to −2°C at Summit Station.

To begin, the summer of 2012 in central North America was one of a prolonged drought and heat wave, the worst since 1895 [Hoerling *et al.*, 2014]. The coincidence of the Summit melt episode with this prolonged summer drought and heat wave over the mid-North American continent led us to investigate a potential causal linkage between these events. To explore this linkage, we carried out a series of analyses of synoptic weather patterns and potential transport paths to Summit Station. Because the most recent prior event of such a scale over Greenland last occurred in 1889, as documented in ice core analyses, we also examined the synoptic environment in the summer of 1889. To do so, we used the recently developed Twentieth Century Reanalysis (20CR) [Compo *et al.*, 2011], which assimilates only surface pressure measurements and prescribes the radiative forcing agents of CO₂, volcanic aerosols, and solar variations, and the boundary conditions of monthly sea-surface temperature and sea ice concentration from HadISST1.1 [Rayner *et al.*, 2003]. Our goal in this latter effort was to explore both the value and limitations of the 20CR in understanding the origins of such extreme events as seen over Greenland in the summers of 1889 and 2012.

2. Factors in the 2012 July Melting Episode

As we will show below, three key factors were present leading up to the 11 July melt episode: (1) the eastward transport of warm air during a record heat wave and drought from the mid-North American continent, (2) advection of water vapor in an Atmospheric River northward over the western Atlantic to the west coast of Greenland, and (3) disturbances in the polar vortex as measured by excursions of the Arctic Oscillation creating an opportunity for transient northward transport of heat and moisture. This northward transport also took place in the presence of warmer ocean waters along the transport path in the northwest Atlantic associated with the positive phase of the Atlantic Multidecadal Oscillation (AMO).

2.1. Trajectory Analysis

Figure 1a shows back trajectories at 00-Z and 12-Z, from Summit Station on 11 July, indicating that the air likely originated in the mid-to-eastern US about 10 days earlier (using the Global Monitoring Division

Table 1. Elevation, Pressure Level, and Temperature for 00 UT and 12 UT Along Back Trajectories From Summit Station Starting on 11 July 2012 at 00 UT and 12 UT

Day	00 UT			12 UT		
	km	hPa	°C	km	hPa	°C
July 11	4.2	603	−7	4.2	603	−7
July 10	4.0	620	−5	3.7	645	−2
July 9	3.4	671	0	3.8	639	−3
July 8	2.8	726	6	3.0	706	4
July 7	2.6	744	8	2.6	747	8
July 6	2.8	721	5	2.1	799	14
July 5	2.8	723	6	1.3	867	21
July 4	2.4	759	10	1.5	857	20
July 3	1.2	879	22	1.5	859	20
July 2	0.5	957	28	1.3	876	22
July 1	0.4	957	29	1.0	900	24

Isentropic Transport Model [<http://www.esrl.noaa.gov/gmd/dv/iadv/>] based on *Harris and Kahl* [1994] and using National Centers for Environmental Prediction (NCEP) meteorological data). We also compared the trajectory analysis in Figure 1a with those derived applying the tool developed by *Noone and Simmonds* [1999] to calculate 700 hPa back trajectories using the NCEP/DOE reanalysis [*Kanamitsu et al.*, 2002], the Climate Forecast System Reanalysis (CFSR, [*Saha et al.*, 2010]), and the Twentieth Century Reanalysis (20CR, [*Compo et al.*, 2011]) as shown in Figure 1b where we also show the temperature anomaly over the eastern US at 925 hPa for 1 July 2012. Based on the consistency of these four methods, it appears likely that the air parcels arriving at Summit on 11 July had a continental origin in North America. In the way of contrast, back trajectory analyses from 2010 and 2011 from Summit Station during temperature maxima showed air mass origins in either the South Atlantic or Europe. Although such isentropic analyses have some level of uncertainty and neglect diabatic processes (e.g., radiative flux divergence, condensation, and evaporation), they paint a consistent picture of the origins of the air impacting Greenland similar to other analyses looking at long range transport of air of continental origin [e.g., *Merrill et al.*, 1985].

The origins of the air parcels in the boundary layer over North America can be seen in Table 1 where we show the daily height, pressure level, and temperature starting from 11 July using the NOAA/GMD analysis for 00Z and 12Z. Note that the temperature of the parcels above Summit Station at 4.2 km ASL (603 hPa), −7°C, if lowered adiabatically 85 hPa to the surface at 688 hPa would warm to about 1°C. We also examined the daily distribution of the trajectories, given the rarity of such melt events. In Figure S1, we show 10 day back trajectories from the CFSR for 00Z (1a) and 12Z (1b) for the month of July 2012. Of note are the origins of most trajectories north of 50°N with a subset clustering along a path from the US east coast over the northwest Atlantic and along the northwest coast of Greenland (as seen in Figure 1 for 11 July). These clusters of trajectories over the western Atlantic suggest a major marine influence on air flowing north to Greenland.

2.2. The Role of Atmospheric Rivers

As has been noted earlier, warm air advection along the Greenland west coast has been identified as a key ingredient in melting at lower elevations on the ice sheet [*Fettweis et al.*, 2013]. Warm air aloft and thin liquid-water clouds were key ingredients in temperatures exceeding the melting point at Summit Station on 11 July 2012 [*Bennartz et al.*, 2013]. One way to transport moisture to this area is through Atmospheric Rivers (ARs). ARs are narrow filaments of water vapor associated with extratropical cyclones; they provide a focused delivery mechanism of moisture from the ocean into continental areas. The potential for such a mechanism gave rise to the question of whether such features were also involved in the 11 July event over Greenland.

ARs are a feature of the extratropics responsible for >90% of the poleward water vapor transport in midlatitudes [*Zhu and Newell*, 1998] and are responsible for extreme precipitation in many coastal regions [*Ralph and Dettinger*, 2012]. ARs are easily identified in SSM/I imagery (Special Sensor Microwave Imager) using the method developed by *Ralph et al.* [2004]. The SSM/I image on 7 July (Figure 2a) shows a concentrated filament with very large values of 4 to 5 cm of integrated water vapor (IWV), which is roughly double the average values of maximum IWV found in summer in ARs over the northeast Pacific [*Neiman et al.*, 2008]. Overlain on the SSM/I image are back trajectories from 11 July at Summit derived from the NCEP/DOE

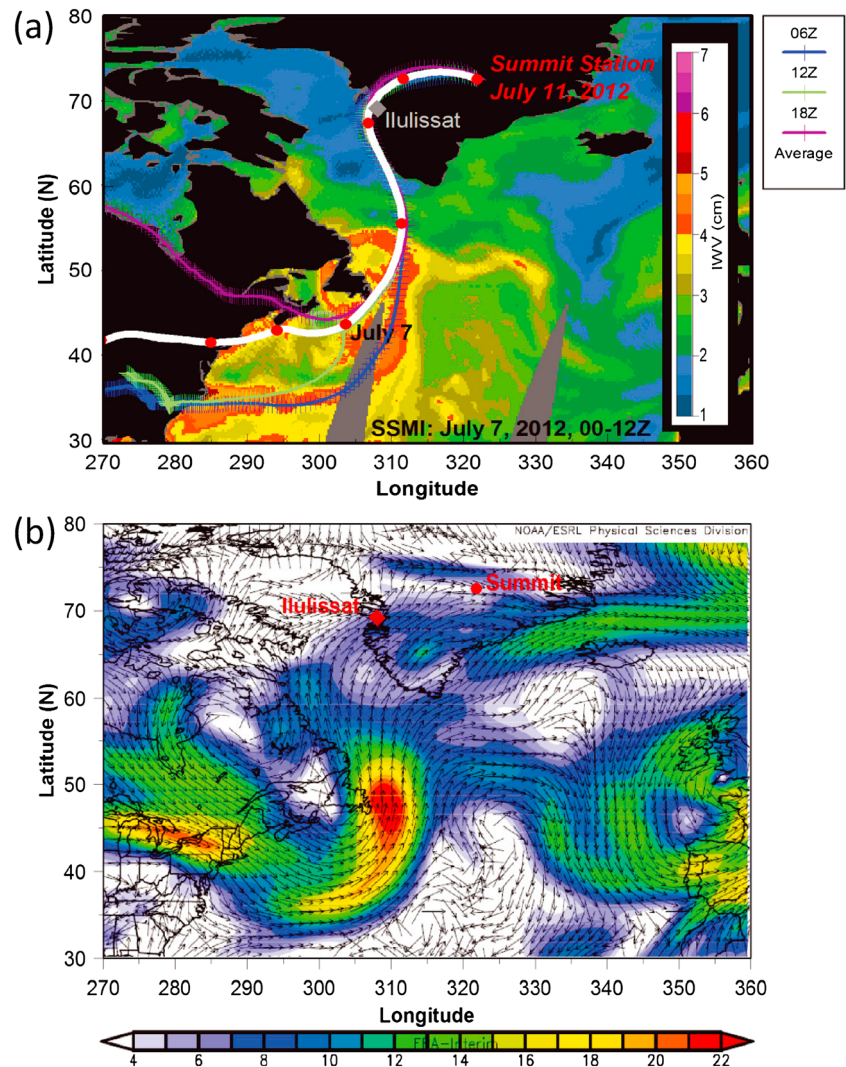


Figure 2. (a) SSM/I image showing the developing atmospheric river (AR) and associated water vapor filaments extending from the US toward the southwest coast of Greenland on 7 July. Individual back trajectories from the NCEP/DOE reanalysis are shown for 06, 12, and 18Z 11 July from Summit Station as well as their average (where the daily interval is indicated by the red circles). Note all the trajectories pass over Ilulissat on the west coast of Greenland. The 11 July-06Z trajectory, on 7 July, overlies closely one of the water vapor filaments. (b) ERA-Interim wind vectors (700 hPa) and speeds (ms^{-1} , scale below) for 7 July.

reanalysis data, which show several individual trajectories as well as their average. Note that the 7 July segment of the 0600Z trajectory overlies the filament seen in the SSM/I image on 7 July. In Figure 2b we show the 700 hPa wind vectors, from the 7 July ERA-Interim reanalysis [Dee et al., 2011], that eventually carry the high IWV air parcels up the west coast of Greenland over Ilulissat on the coast and thence to Summit Station (note that the pressure at Summit Station during this period was about 680 hPa so 700 hPa is the closest standard level in the reanalysis: it should be noted that in reanalyses, variables are typically interpolated below actual terrain elevations). In Figure 3, the sequence of SSM/I images shows that the high-vapor portion of the AR reached southern Greenland on 8 July and continued to direct water vapor along the west coast of Greenland through 10 July. By 12 July the very-high IWV air had moved away from Greenland but extended eastward across the Atlantic to northern France and southern England where heavy rains resulted [cf. Lavers and Villarini, 2013]. Although ARs are most recognized for their role in water vapor transport and precipitation during the cool seasons [Ralph and Dettinger, 2012; Ralph et al., 2005], they also occur in the summer [Neiman et al., 2008]. It is clear from this case that they can play a role in summer both for Greenland and for the European coast. It should also be noted that during this period the AMO was in its positive phase, with ocean surface

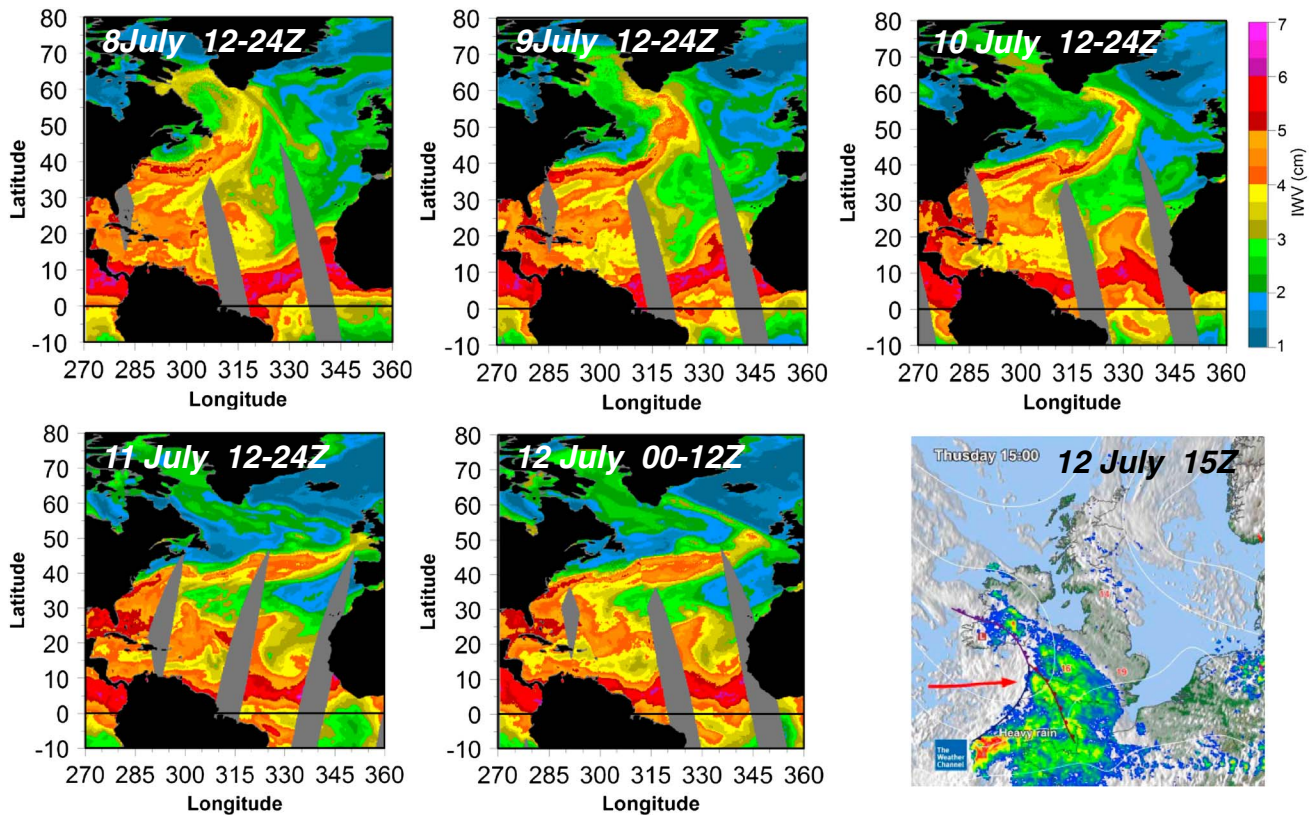


Figure 3. Sequence of SSM/I images (10°S–80°N, 270°E–360°E) following the progression of the AR from when it first impacts Greenland until it makes landfall in France and England (far lower right: <http://uk.weather.com/partners-JulyOutlook/71212forecast>). IWV scale at the upper right is from 1 cm to 7 cm). Note the residue IWV left along the west coast Greenland following the AR transition to the east.

temperature anomalies just south of Greenland in excess of 2°C during June and July 2012 (Figure S2a), suggesting a potential role in enhancing the warm and humid anomalies in the northward flow indicated in the 1000 hPa vector winds shown in Figure S2b. By way of comparison, studies of the effect of warm near-shore ocean waters along the California coast, using direct flux measurements by research aircraft, have shown that increased boundary layer latent and sensible heat fluxes can both destabilize the adjacent atmosphere (promoting increased vertical mixing) and increase the moisture content of onshore flow in an AR [Persson *et al.*, 2005]. In Figure S2b, the wind vectors also reveal the cyclonic circulation centered over the coast of Newfoundland and the anticyclonic circulation centered over the southeast coast of Greenland that together facilitate the flow along the west coast of Greenland and onto the ice sheet.

2.3. Disturbances of the Large-scale Polar Circulation and Transport

Figure 4 shows the time series of 2 m temperature at Summit Station and indices of the Arctic Oscillation (AO) and North Atlantic Oscillation (NAO) through the summer. The time series in Figure 4 indicate a fairly variable polar vortex, as measured by the AO index but not the NAO index, during the summer of 2012. It is apparent that the first two multi-day warmings follow a negative to positive excursions of the AO by 1 to 3 days (whereas the NAO remains in a relatively negative phase for most of the period). The rapid warming on 29 July starts following a major transition from a positive AO to a negative one, suggesting that it is the transition in the state of the AO that presages increased southerly flow into the Arctic. These variations of the AO are consistent with increasing amplitude of trough-ridge patterns that favor transport of warm air from the south between the low- and high-pressure centers. Because the AO is well established as an important feature of the wintertime northern hemisphere circulation but much less so in the summer, its extremes in the summer of 2012 suggest its importance to summer circulation anomalies that influence Greenland melt episodes: In this context it is the changes in the polar circulation, perhaps as indicated by changes in the AO index, that provide the transients in the southerly transport of warm, humid air along the west coast of Greenland and thence over the ice sheet.

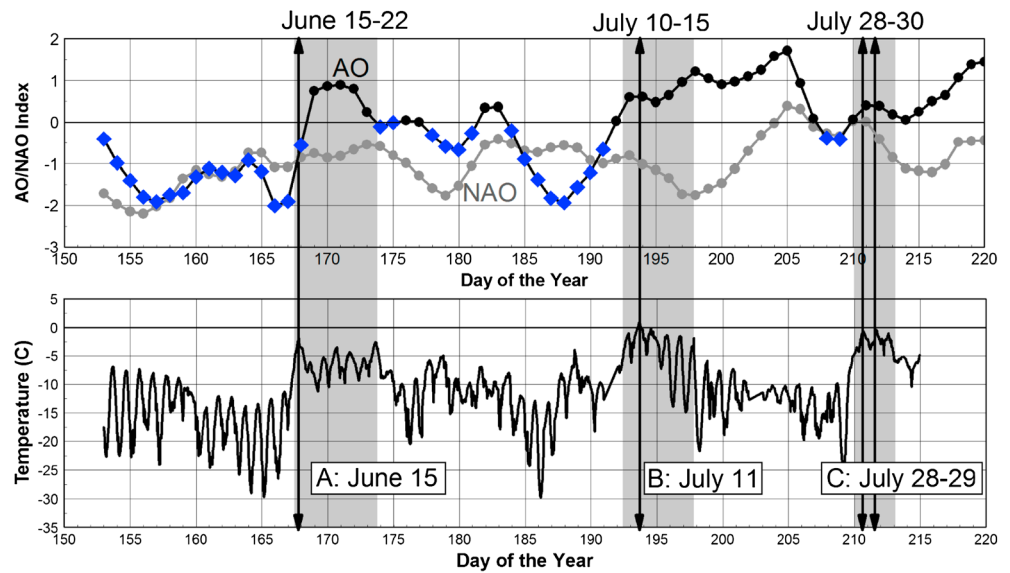


Figure 4. Upper: Time series of the Arctic and North Atlantic Oscillations (AO, NAO) for the summer of 2012. Negative values of the AO are highlighted in blue. Lower: Temperature time series from Summit Station showing three major warm periods (Labeled A, B, and C for later reference) highlighted in gray (data provided by NOAA ESRL/Global Monitoring Division). In each case, the warming follows a transition from negative to positive AO. Temperature extrema in each warm period are indicated by vertical lines: Dates of maximum temperatures are labeled. The NAO shows no clear signature relative to the warmings.

Leading up to the major melt episode on 11 July, a well-defined trough-ridge pattern developed with significant northward transport of warm, moist air along the west coast of Greenland (see Figure 2b). This event was also characterized by a rapid transition from a Wave-Six pattern (with high geopotential height (GPH) over the Arctic Ocean and six centers of low GPH at lower latitudes: one trough, in particular, lies just west of Greenland on 5 July) to a simple Wave-One pattern with a moderately positive AO on 12 July expressed as low GPH over the Arctic Ocean and high GPH over Greenland (Figure S3). While blocking events often favor warm episodes over Greenland in concert with a positive AMO [Hanna et al., 2013], we have found that the eastward shift of the anticyclonic ridge, often to the southeast coast of Greenland, is what favors the transient transport of warm humid air northward along the west coast of Greenland (as will be seen in Figure 6). It should also be noted that a highly negative AO was an antecedent to the rapid warming that led to the 11 July melt episode. This suggests that extreme warming events such as that in 2012 originate from a transient event, rather than a persistent high pressure pattern over Greenland. The coincidence of the warming episode with a transition in the state of the AO suggests that examining the predictability of such rapid transitions in polar vortex behavior and their representation in weather and climate models may be worthwhile. Such results are also consistent with recent efforts in the analysis of climate models that examine whether a Wave-Five pattern can provide a longer-range predictor of continental heat waves over the US. [Teng et al., 2013]. In fact, a Wave-Five pattern in the 0.2582-sigma (about 250 hPa) streamfunction appears on 8 July just prior to the melt episode on 11 July (Figure S4). Limits on the predictability of the excursions in the AO prior to the 11 July event can be seen in Figure S5 where the Global Forecast System (GFS) ensemble mean and spread forecasts from the NOAA/NWS Climate Prediction Center are seen at 7, 10, and 14 days for the summer of 2012. These results suggest significant skill at 7 days but not at 14 days when climatology prevails and little forecast skill remains for the vicinity of Greenland. Given the limited predictability of the GFS, and potentially other global models in the polar regions, such results should provide limits on any future advance planning of intensive field programs studying such extreme events.

2.4. Transport Details

In the previous section we showed that the major transport path for warm humid air arriving at Summit Station was along the west coast of Greenland (cf. Figure 1). This transport path required a ridge-trough pattern with the ridge of high pressure favoring the southeastern side of Greenland and a trough to the west

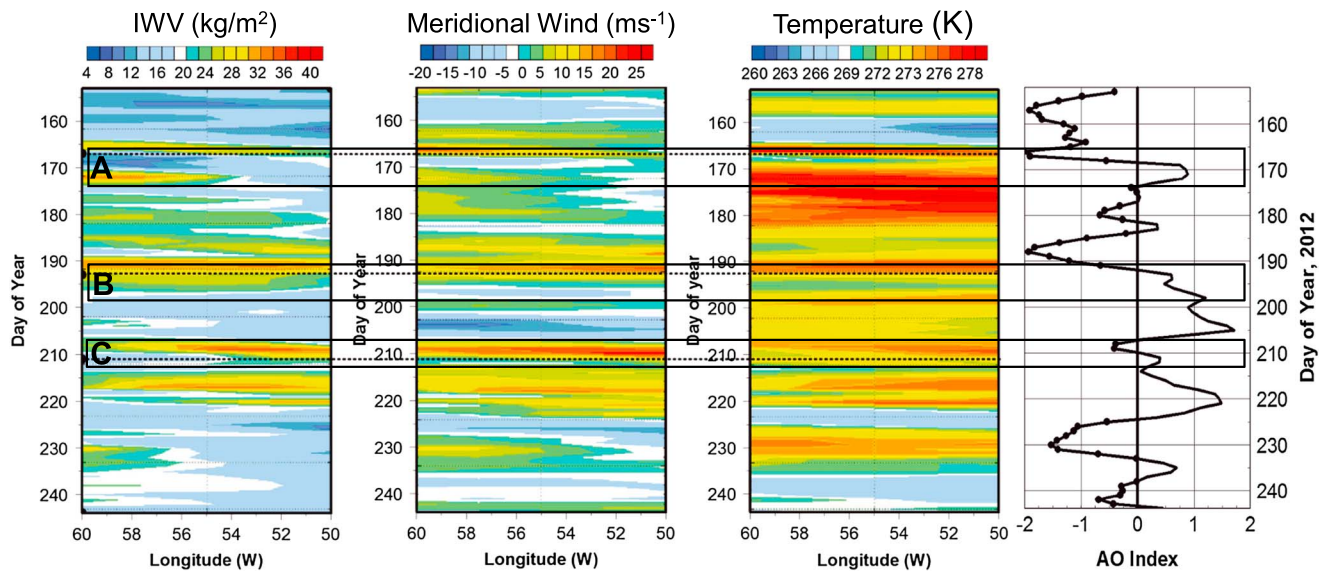


Figure 5. Hovmöller (time-longitude) cross sections of integrated water vapor (IWV, kg/m^2), meridional wind (ms^{-1} , 700 hPa), and temperature (K, 700 hPa) for the summer of 2012 just west of Greenland between 50°W and 60°W and averaged from 60°N to 65°N . Three warming periods (A, B, C) are indicated by the boxed areas and correspond to the periods of maximum temperature at Summit shown in Figure 4. Dashed lines indicate the times of maximum temperatures for each case at Summit which are later than the increases at the west coast. The time series of the Arctic Oscillation (AO) to the right provides a comparison of each event with rapid changes in the state of the AO.

toward Baffin Island and Newfoundland (cf. [Hanna *et al.*, 2013], their Figure 7g). Looking in more detail at the summer of 2012, Figure 5, using the NCEP/DOE reanalysis, compares the three warm periods of 2012 with Hovmöller diagrams for the period of June through August (days of the year: 153–244) of vertically integrated water vapor (IWV), meridional wind, and temperature at 700 hPa (latitudinally averaged between 60°N and 65°N and displayed between 60°W and 50°W , which is the extent of Davis Strait). Periods of maximum temperature at Summit identified in Figure 4 are also labeled A, B, and C to compare the IWV, lower tropospheric wind and temperature, and the AO index. In Case A, very warm temperatures prevail west of Greenland for almost 2 weeks. However, there is no northward transport of water vapor except on the west side of Davis Strait. In Case B, just prior to the major melt at Summit on 11 July, winds in excess of 15 ms^{-1} carried warm and high-water-vapor air along the west coast of Greenland. This transport path extended over the entirety of Davis Strait. In Case C, warm, moist air was largely confined to the eastern side of Davis Strait. In the time series of the Arctic Oscillation, it is evident that major changes in the AO index (positive and negative) are associated with warm air advection to Greenland. This argues that the extreme events in the summer of 2012 over Greenland are associated with transients in the large-scale polar circulation.

The associated IWV patterns and 500 hPa GPH fields from the GFS for each case (for 2 days prior to each temperature maximum) are cross-referenced in Figure 6 with SSM/I imagery to provide an estimate of the fidelity of the GFS in producing appropriate maps of IWV. From these figures it appears that the GFS is slightly drier than observed in the SSM/I images by 20–30%. The spatial patterns in Figure 6 are also consistent with the distribution of IWV across Davis Strait shown in the Hovmöller diagrams in Figure 5. It should also be noted that the SSM/I image and GFS output for 13 June show that the major transport path for water vapor northward was over continental areas rather than the ocean south of Greenland as is the case for 9 and 27 July. In the 500 hPa patterns on the right of Figure 6, a major distinction lies in the position of the trough-ridge couplet. On 13 June, the center of low GPH is over Hudson Bay and the ridge of high GPH lies over Davis Strait whereas for both 9 July and 27 July, the low GPH center extends to Labrador and the high GPH ridge intersects southeast Greenland. For both 9 and 27 July, the orientation of the isopleths of GPH is consistent with transport along the west coast of Greenland.

We have argued above that the major melt episodes in July 2012 followed transport of warm humid air via ARs to the west coast of Greenland. Back trajectory analysis suggests that these air masses then moved over Ilulissat on the Greenland coast and thence to Summit Station (cf. Figures 1 and 2). It has also been argued

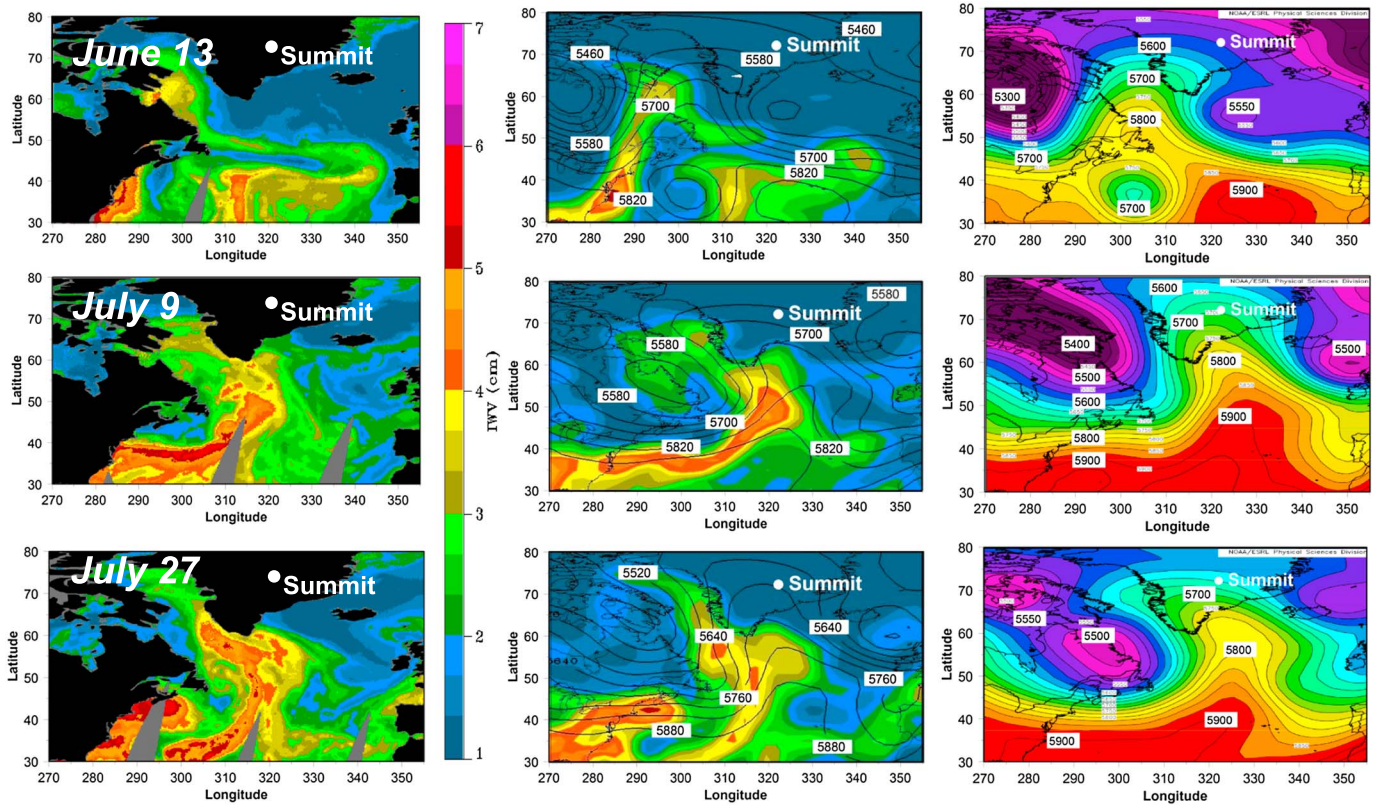


Figure 6. Comparison of (left) SSMI-derived IWV with that from the (middle) Global Forecast System (GFS) analysis and (right) 500 hPa height fields. Scale is the same for both IWV products. *Top left:* 13 June 12–24Z: The observed and reanalysis-derived IWV show low-total vapor near Greenland. *Middle left:* 9 July 00–12Z: Strong northward transport, as indicated by the GPH field (right figure), of relatively moist air. *Bottom left:* 27 July 00–12Z: Strong northward transport of relatively moist air. The observed IWV (left) shows more significant vapor transport to the north along the west coast of Greenland. In all three cases the GFS provides a close approximation, but is slightly drier, compared to the IWV derived from the SSMI. The 500 hPa contours on the right are at 25 m intervals from 5450 m to 5950 m. Note that on the warmest days at Summit the ridge axis intersect the southeast coast of Greenland. On 13 June, the ridge is aligned west of Greenland, and the moisture plume lies largely over land areas. Note that on the second two days the high IWV areas align along the more closely packed contours over the north Atlantic.

[Bennartz *et al.*, 2013] that the critical ingredients in the 2012 melt at Summit Station were the presence of both warm air aloft and a thin liquid cloud layer to enhance the radiative warming of the surface. For the warmest day in each of the three cases we identified in Figure 5, we examined daily time-height sections of the Summit millimeter cloud radar reflectivity (Figure 7). In Case A, in mid-June, 700-hPa temperatures were the warmest of the summer west of Greenland but northward transport was weak with little IWV along the coast. A relatively thick mixed-phase cloud with significant ice-crystal precipitation, as seen in the cloud radar reflectivity, was present over Summit Station consistent with colder air aloft, in agreement with the colder temperatures seen in the daily radiosonde profiles (not shown). For the 11 July melt episode (Case B), significant northward transport of IWV is present with a ridge axis a bit further to the east, enhancing the northward transport of water vapor over the ocean. The cloud radar shows the thin elevated liquid-water cloud, together with warmer air aloft, identified in Bennartz *et al.* [2013] in the afternoon hours which contributed to the enhanced heating in the boundary layer. The absence of ice-crystal precipitation later on 11 July (i.e., low reflectivities) supports the contention that both warm air aloft and a small amount of cloud liquid water are present to optimally enhance the surface warming through the combined effects of downward solar and long-wave radiation [Bennartz *et al.*, 2013], unlike the situation in June. In this case, we hypothesize that the northward advection of both warm and humid air along the west coast set the stage for transport and formation of liquid cloud layers over the interior of Greenland. For example, cyclogenesis in the area of Baffin Bay is known to enhance snow accumulation with southwesterly flow into the west coast of Greenland during winter months [Rogers *et al.*, 2004]. However, many of the analyses of summer anomalies have been on blocking events [e.g., Overland *et al.*, 2012] rather than on the troughs that develop west of Greenland that can enhance southwesterly flow onto the ice sheet.

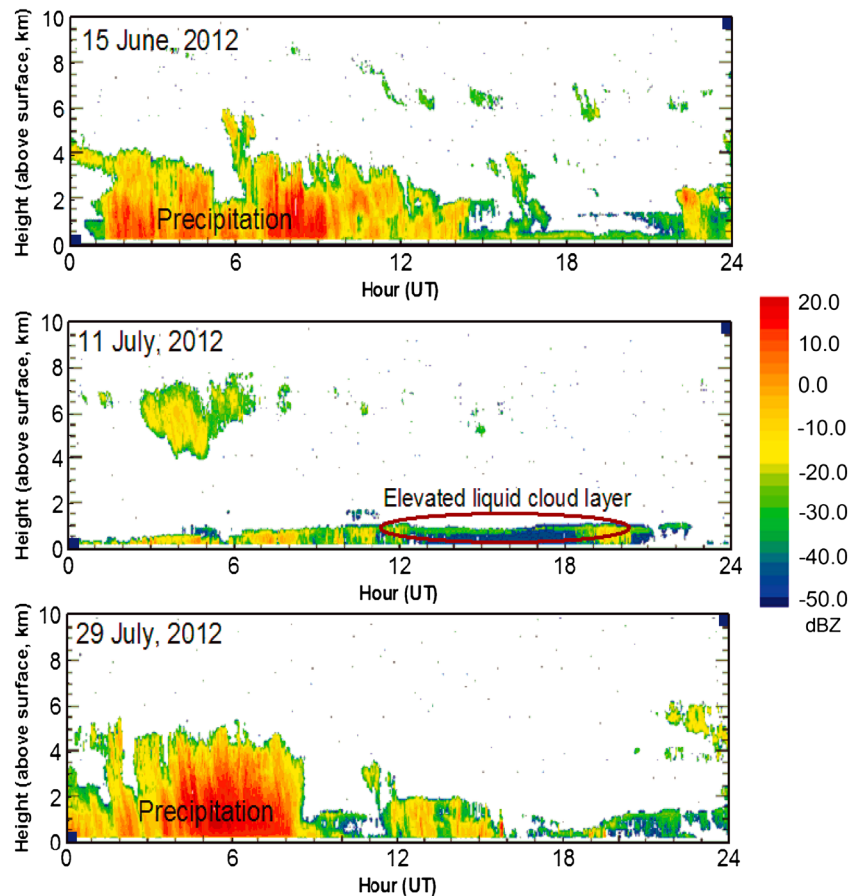


Figure 7. Millimeter Cloud Radar reflectivity using ICECAPS data for 15 June (Case A), 11 July (Case B), and 29 July (Case C). The reflectivity scale is to the right. Note the low reflectivity on 11 July from the liquid layer cloud compared to the regions of precipitation (ice crystals).

Some insight may also be suggested from recent studies such as that of *Kingsmill et al.* [2013] who demonstrated that Atmospheric Rivers encountering topography can override shallow barrier jets such as those that form just west of the Sierra Nevada and deliver their moisture to the upper Sierra, a scenario that would be plausible in Greenland as well and worth further study. The isentropic analysis of trajectories riding over Greenland (cf. Table 1) supports such a mechanism. In Figure S6 we show the time series of wind direction and temperature over a 5 day period leading up to and following the melt episode. During the periods of maximum warming on the 10th and again on the 11th, the wind is from the west to northwest consistent with transport from the west coast of Greenland. From the 12Z rawinsonde profiles on the 10th and 11th, the wind aloft above Summit rotated from west-northwest to northerly (not shown, available from the ICECAPS web site). Two features are notable in Figure S6: (1) a temperature increase at Summit from -25°C on 9 July to above freezing on 11 July, (2) this follows the increase in meridional winds from the south developing along the west coast of Greenland (Figure 5) coincident with the rapid warming and consistent with the back-trajectories shown in Figure 2 and the water vapor transport in Figure 6.

In Case C, late in July during the partial melt on 29 July, significant northward transport is again present along the west coast with the ridge axis again a bit to the east and south of Greenland. In this case, the cloud radar shows a thicker precipitating layer overnight with more intermittent periods of cloudiness and elevated thin cloud layers during the remainder of the day. In Case C, cloud temperatures are 2° to 3°C cooler than on 11 July (not shown). In addition, a number of the back trajectories originate either in the Caribbean and/or the southern Atlantic rather than over the North American continent where temperature anomalies were also less persistent. These less favorable factors may have been an important part of the reduced melting during this case. In addition, coastal observations at Ilulissat showed a maximum temperature of 17°C on 27 July, 2 days

prior to the near melt on 29 July, accompanied light rain and fog. This compared to a maximum temperature at Ilulissat of 21°C on 10 July with light rain recorded on 9 July (<https://weatherspark.com>).

3. Comparison With the Last Summit Melt Episode in 1889

The last extensive melting of the high Greenland ice sheet prior to 2012 occurred in 1889 as measured in an ice core near the current Summit Station [Meese *et al.*, 1994]. We have hypothesized and found evidence that the 2012 melting event was accompanied by a rare combination of (1) the eastward transport of warm air during a record heat wave and drought from the mid-North American continent, (2) followed by disturbances in the polar vortex as marked by transitions in the Arctic Oscillation leading to an increased likelihood of transient northward transport of heat and moisture, and (3) the presence of an Atmospheric River transporting water vapor northward over the western Atlantic to the west coast of Greenland and thence onto the ice sheet. We also noted that the Atlantic Multi-decadal Oscillation was in its positive phase with warmer ocean waters south of Greenland. Here we examine the summer of 1889 using the 20CR and other documentation to diagnose whether these same factors may have been present during the 1889 melt episode(s) and to determine the possible timing of the melt guided by key factors found in the 2012 event(s). Because the 20CR uses an Ensemble Kalman Filter data assimilation system [Compo *et al.*, 2011; Whitaker and Hamill, 2002], a measure of uncertainty is given by the ensemble standard deviation or spread of the 56 members of the analysis. The system generates an estimate of the state of the atmosphere (e.g., winds, temperature, and humidity) and the uncertainty in that state every 6 h. Typically, in the summer of 1889, the ensemble spread fields for temperature and GPH at 500 hPa suggest the more reliable results for examining larger scale dynamics occur over southern Greenland, over ocean areas and over the mid-continent (e.g., Figure S7). Because there are only sparse observational data with which to compare 20CR results, we primarily looked for coherent patterns and temporal consistency in the results, and compared with the limited surface data available for that era.

3.1. Resolving the Likely Time(s) for the Melt Event in 1889

One of the challenges facing any interpretation of the 1889 event is that the ice core record from Summit does not allow the timing (month/dates) of the summer melt in 1889 to be resolved and daily meteorological data are limited to just a few coastal stations. However, because of the association of the melting events in 2012 with northward transport of heat and moisture along the west coast of Greenland, we looked at daily time series from 20CR using a grid point near the Ilulissat weather station (69.23°N, 51.07°W, also named Jakobshavn in early records).

To start, we examined the 2 m minimum temperature from 20CR and minimum observed Ilulissat station temperature after removal of their mean values in Figure 8a (maximum temperature data were not available from Ilulissat in the 1880s nor were daily data available from other sites on the west coast of Greenland). For the June–July–August temperatures, the 20CR average minimum temperature was 0.78°C compared to an observed average from Ilulissat of 3.03°C, consistent with the ensemble spread associated with the 20CR. (The 20CR ensemble spread in 2 m air temperature ranged from about 2°C around the coast of Greenland to 6°C near the location of the current Summit Station (Figure S8). The absence of surface pressure data for this area suggests that the 20CR results are dominated by oceanic SST data and weather information propagated from the nearby, well-observed continental regions during these summer months.) The 20CR also captures a decent fraction ($r^2 = 0.3$) of the variability in the 3 month observed temperature time series, which may be surprising, especially given the comparison of a point measurement with an estimate from the ~2.0° grid resolution in the 20CR.

The major summer maxima in northward transport of moisture over Ilulissat can be seen in the 20CR 850 hPa meridional wind (Figure 8b), and the 20CR integrated water vapor (IWV) (Figure 8c). There are two pronounced maxima in IWV beginning on calendar days 186 (5 July) and 211 (30 July) that correspond to the two maxima in northward transport. There is also an excursion in the Ilulissat temperature on calendar day 197 (16 July): In this case, a trough-ridge pattern formed, similar to that preceding the 11 July 2012 event, but with a minor moisture anomaly diagnosed by the 20CR of only 3 kg/m² (compared to an anomaly of 10–20 kg/m² in 2012). Figures 8d and 8f show the coherent spatial distribution evident of IWV on the days of major northward transport with an AR moving northward on the eastern edge of the trough, along the east coast of North America and then along the west coast of Greenland. Figure 8e shows the pattern on Day 197 when the 20CR does not show the moisture plume reaching the west coast of Greenland,

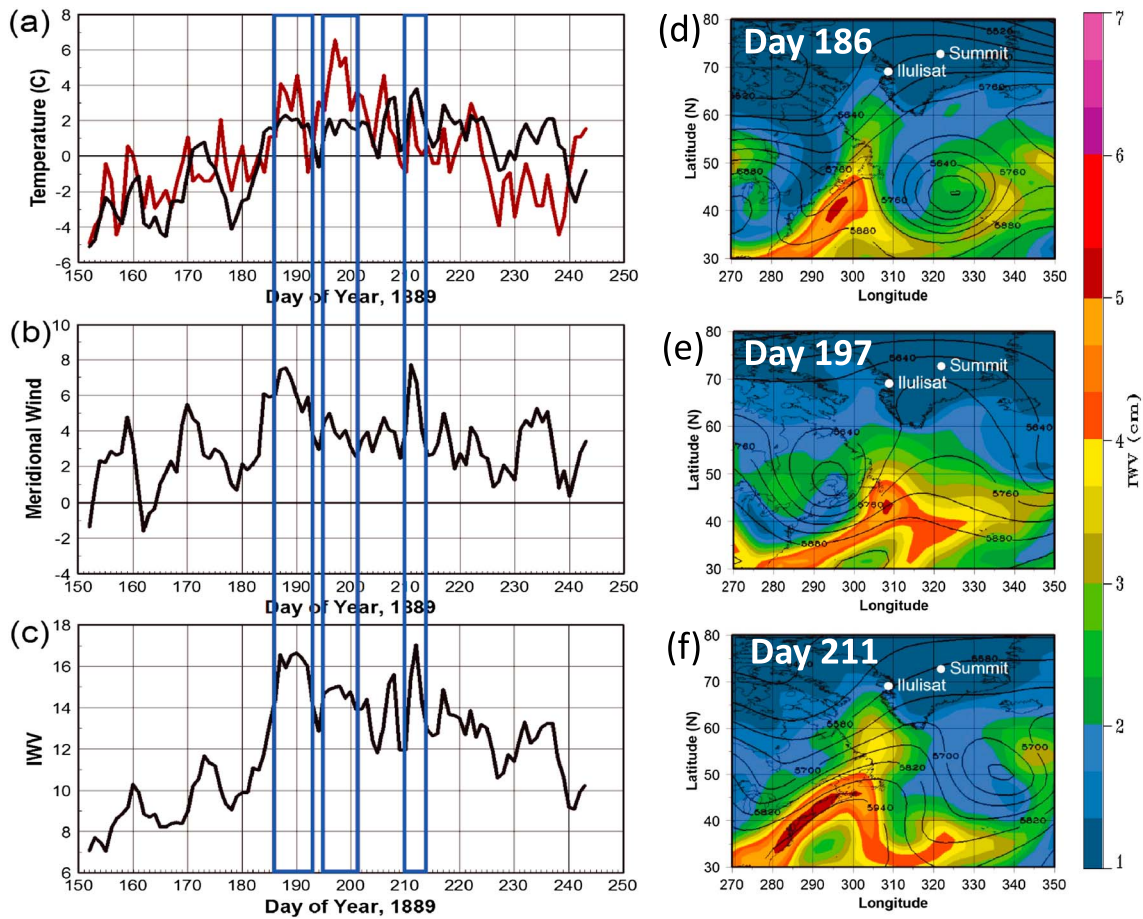


Figure 8. Left: (a) Time series of 2 m minimum temperature at Ilulissat for the summer of 1889 from the 20CR (black) and the local weather station (red), (b) 850 hPa meridional wind from the 20CR at the location of Ilulissat, and (c) integrated water vapor (IWV) above Ilulissat. Three event periods are indicated by the blue boxes where there was either a maximum in temperature and/or strong northward movement of IWV. Right: Snapshots of IWV from the 20CR on Days (d) 186, (e) 197, and (f) 211 during the event periods identified on the left. Dark red areas of IWV represent total column water vapor of over 5 cm seen in the scale on the far right. Contour interval (500 hPa) is 60 m.

although the trough-ridge pattern is most similar to those on 9 and 27 July 2012, prior to the melt episodes (Figure 6). Consistent with this inferred transport pattern, precipitation at Ilulissat station was observed on 5 July and again intermittently from 21 to 30 July (not shown). During the temperature maximum on 16 July, there was no evidence of a significant AR nor recorded precipitation (cf. Case A, Figure 5 for 2012).

In contrast to 2012, a well-established Bermuda High was present on 30 July and to a lesser extent on 5 July 1889. In comparing 1889 with 2012, it appears that the effect of the Bermuda High in 1889 was to shift the path for water vapor transport somewhat to the west along the eastern seaboard of North America. The year 1889 was also somewhat different as a low pressure system had descended southeastward from the Labrador Sea and had produced a deep cutoff low just to the northwest of the Azores: This synoptic setting with large latitudinal and longitudinal gradients made the back trajectory analyses sensitive to their starting location and timing south of Greenland.

We also examined time series of temperature at 700 hPa above the southern tip of Greenland (60°N, 45°W) and over the location of the current Summit Station (Figure S9). These show the first temperature maximum occurring in early July, at 700 hPa on Day 187 above the southern tip of Greenland (about the same day as at the Ilulissat weather station) and slightly later on Day 189 over the location of the present day Summit Station. Near-surface temperatures, close to the Summit Station location, appear substantially cooler in the 20CR than those further south, although the maxima are similar in timing and the difference is within the range of the ensemble spread of the 20CR results (6°C, Figure S8). From the time series in Figure S9, the warming during days 186–193 is the longest and most pronounced of the three potential events in 1889.

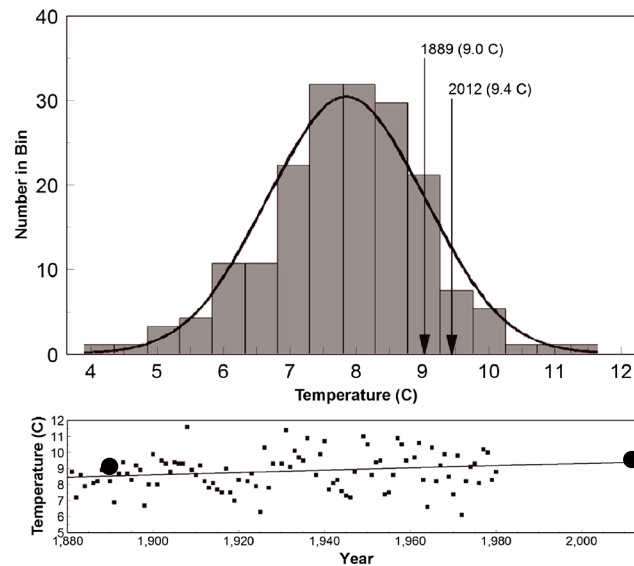


Figure 9. (a) Distribution in 1°C bins of monthly averaged July temperatures from Ilulissat based on *Vinther et al.* [2006] where their processing used infilling from adjacent stations. The data included 174 months between 1807 and 2005. (b) Time series of July monthly Ilulissat temperatures from http://data.giss.nasa.gov/gistemp/station_data/ and least square fit line. Monthly temperatures for 1889 and 2012 are shown by the solid circles.

Another question concerns whether 1889 was unusual in the context of adjacent years. For example, longer time series from Greenland coastal weather stations [*Vinther et al.*, 2006] show that 1889 was not substantially warmer compared to other years in the late 1800s. This suggests that the melt episode in 1889 may not have been due to any anomalous warming period. Also intriguing is the fact that the period in the late 1880s was one of the coolest on record for annual Greenland surface temperatures [*Box et al.*, 2009].

However, in terms of monthly July temperatures, the entire record at Ilulissat shows no significant long-term trend from 1880 to 1980. In fact, the monthly average temperature at Ilulissat for July 1889 was 9.0°C, whereas for July 2012, it was 9.4°C. Figure 9 summarizes this July-temperature history at Ilulissat using the long time series of monthly averaged temperatures from *Vinther*

et al. [2006] in a frequency distribution. These data started in 1808 and were in-filled based on regressed values from other coastal sites [*Vinther et al.*, 2006]. We also examine in Figure 9 the raw monthly time series for July using data available from NASA (http://data.giss.nasa.gov/gistemp/station_data/) for the period 1881 to 1980. Although linear regression only accounts for 3% of the variance, there is a long-term trend discernible in the time series. From Figure 9 where we have indicated the raw monthly temperatures from Ilulissat, it is clear that monthly temperatures for 1889 and 2012 are both well away from the wings of the distribution of monthly temperatures and are thus not likely to be associated with persistent and extreme local heat anomalies. Although in the 1880–1980 time series there is a weak upward trend, there also appears to be a step increase around 1925.

3.2. Trajectory Analysis

Based on the preceding analysis, we looked further at the days 5 July and 30 July as potential dates for the 1889 melt event(s) based on the higher likelihood of moisture transport to the west coast of Greenland associated with AR-like plumes appearing in the 20CR, observed maxima in temperature at Ilulissat on those days, and strong meridional transport.

When we examined the use of the 20CR derived back trajectories from above the ice sheet, they showed mostly terrain-dominated flow (terrain-following flow and occasionally, what appeared to be topographically trapped eddies—in both 1889 and 2012)—perhaps these were an artifact of the absence of pressure observations over the ice sheet with which to constrain the data assimilation. However, when we started the 20CR back trajectories just offshore to the west of Greenland along the trajectories found in CFSR and NCEP/DOE Reanalysis in 2012, 20CR produced consistent results. For this reason, we used the 20CR-derived back trajectories for 1889 to determine the origins of air masses arriving near Greenland in the vicinity of AR-like water vapor structures off the southwest tip of Greenland.

The trajectories in Figure 10a use a starting point of 60°N, 50°W (as for the 2012 case) on 5 July 1889 and extend back to 25 June. These show low-level (925, 900, and 800 hPa) trajectories originating in areas south of Hudson Bay and in the upper Midwest where temperature anomalies at 800 hPa of more than 10°C existed. Air parcel trajectories arriving at 700 and 600 hPa originated along the southeast coast of North America. The lower-level trajectories are consistent with the higher pressure over the central US and east of

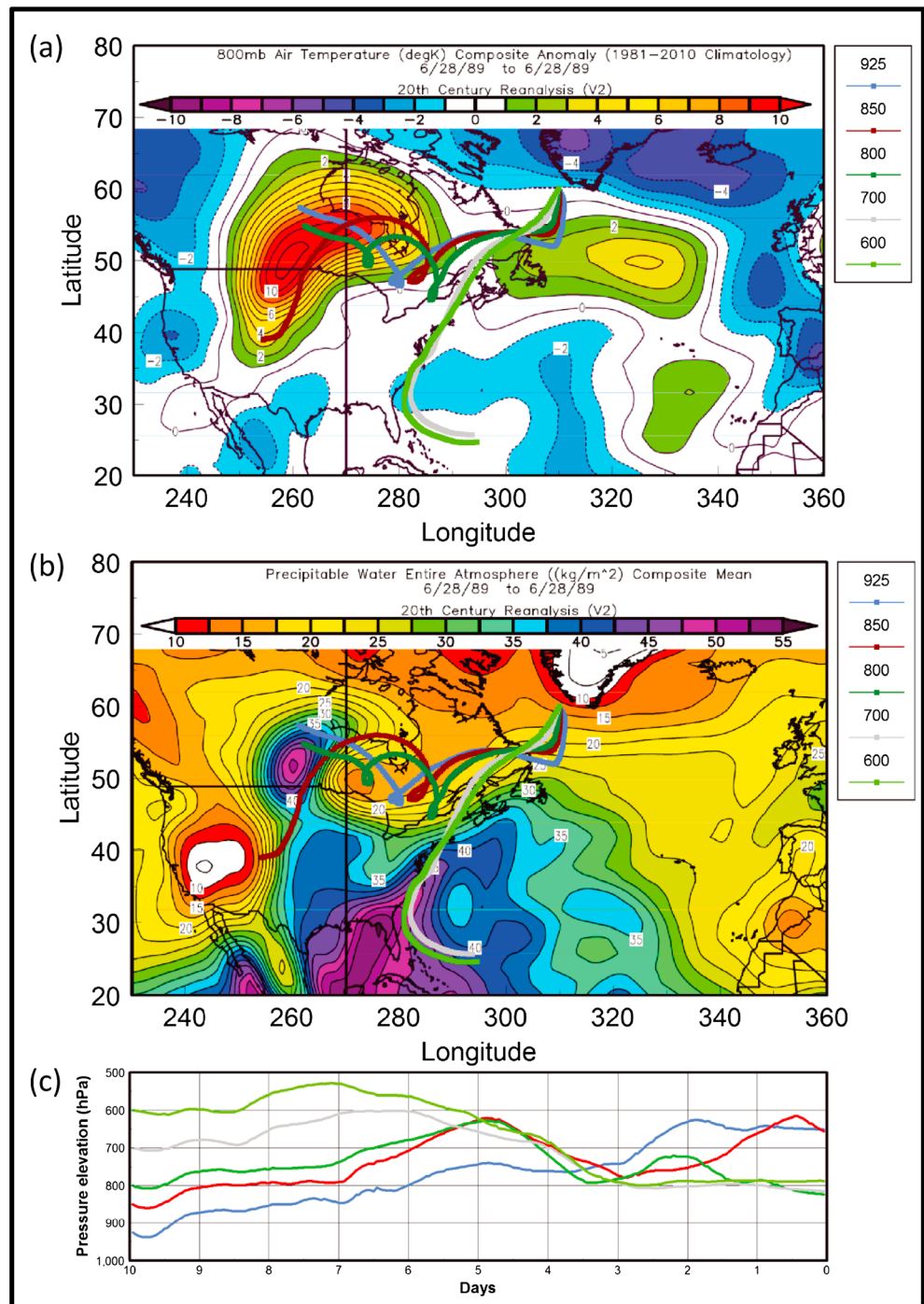


Figure 10. Precursors to the 5 July 1889 temperature maximum at Ilulissat: (a) 800 hPa temperature anomalies with 1.0°C contours on 28 June and associated air trajectories showing transport of warm air at lowest levels from the heat anomaly just southwest of Hudson Bay and along the Canadian border to the Greenland coast and transport along the US east coast. (b) Map of IWV on 28 June 1889 with 2.5 kg/m² contours with transport at upper levels from the southwest Atlantic. (c) Trajectory elevations along isentropes: Note that a number of the trajectories originate either in the heat anomaly or moisture anomaly.

Greenland and with a 700 hPa trough positioned over eastern Canada extending into Newfoundland. Higher level trajectories along the east coast of the US followed the contours of the Bermuda High just to the east. The pressure elevations of the isentropic trajectories all originated at levels of about 800 hPa over the midcontinent as well as in the tropics. These results are consistent with our hypothesis that

preconditions necessary (but not necessarily sufficient) for melt episodes in 2012 and 1889 include a confluence of warm and humid air masses along the west coast of Greenland and warm air trajectories that originate in areas of regionally extreme temperatures over North America.

For the second potential event on 30 July, similar results were obtained for trajectories originating from (60°N,50°W) (Figure S10). Major differences include (1) The majority of trajectories lie primarily in the northern US and southern Canada where the 950 hPa temperature anomalies are weaker; only a few of the trajectories originate in the south central US where the 950 hPa temperature anomaly is less than 5°C, (2) In contrast to 5 July, all but the 925 hPa trajectory originate near the surface for the first 7 days of transport, and (3) The 600 and 700 hPa trajectories arriving at (55°N,55°W) originate in moist tropical areas off the southeast coasts of the US. In comparing continental temperature anomalies prior to 5 July and 30 July, those in the earlier case are much larger and persistent than in the latter case. Together, these results suggest that the July 5 event recorded at Ilulissat most likely preceded by a few days (as in 2012) the melt episode recorded in the ice core near Summit in 1889.

3.3. The Synoptic Environment

Finally, there is the question of the behavior of the polar vortex in 1889. Figure S11 shows the AO Index, an indicator of the vortex behavior, along with the meridional wind, V , at 800 hPa just to the west of Greenland. Of note in the figure are the increases in meridional wind following major changes (positive and negative) in the AO index. In 2012, we found that the major warming on 11 July 2012 followed a recovery from a quite negative AO with an associated Wave-Six pattern. In 1889, the major warming identified in Figure 8 beginning around Day 186 and continuing through Day 194 is initiated as the AO index decreases in concert with increasing southerly winds along the coast of Greenland as shown in Figure S11. Later warming seen in the 20CR on Day 211 corresponds to coincident increases in the AO from negative to positive with, again, increasing southerly winds. In this respect, the AO index appears useful in identifying changes in the state of the polar vortex that can lead to increased advection, at times, of warm, humid air.

It should also be noted that in 1889, the AMO also appeared to be in its positive mode (Figure S12) with a positive anomaly south of Greenland of about 1°C. In the summer of 1889, the AMO index was decreasing from its spring maximum of +0.34. However, residual warm water remained south of Greenland. This compares with an anomaly of more than 2°C in 2012 (Figure S2) in the same region but also extending into the Labrador Sea in 2012. In 2012, the AMO index was increasing through the summer to a maximum of +0.48 in September. In Figure S12, the SST pattern in the equatorial Pacific in July 1889 is that corresponding to the “perfect ocean for drought” in North America (with a cold eastern equatorial Pacific and warm western Pacific south of Japan) [Hoerling and Kumar, 2003] and the optimal SST forcing for drought [Shin et al., 2010].

3.4. Underlying Factors and Other Evidence

Another key factor we identified for the 2012 melt case is the continental North American drought and associated heat wave. The summer of 1889 was also a time of extreme summer drought in the Dakota Territory as well as one of extensive heat and forest fires across the Northwest southern Canada and upper Midwest as documented in accounts describing that era [Arno and Allison-Bunnell, 2002; Kepfield, 1998]. Similarly, Figure S13 shows the tree ring reconstructed annual drought for 1889 from the North American Drought Atlas [Herweijer et al., 2007]. It shows extreme (annual) drought in the upper mid-west and Canada as well as the northwestern US. Although this area of drought is further north and west than in 2012, back trajectories also originate further north. It has been argued by others that forest fires in boreal regions and mid-North America can be a source of black carbon (BC), which can affect the surface albedo and accelerate melting in the polar regions [e.g., Sand et al., 2013].

The role of BC may confound interpretation of the 1889 event because the source regions for the trajectories that we identified for 5 July might include the concomitant influences of both heat and fire during that summer [e.g., Arno and Allison-Bunnell, 2002]. In fact, the Director of the US Geological Survey having traveled across the northern US from the Dakota Territory to the Pacific Northwest in the summer of 1889 reported to Congress that the smoke was so thick that the mountains could not be seen during the entire trip [Arno and Allison-Bunnell, 2002]. Similarly, analysis of the historical fire extent in Jasper National Park in Canada

concluded that the fires of 1889 were the greatest in the history of the park from 1665 to 1971 and closely associated with extreme drought [Tande, 1979]. Interestingly, results from an ice core at D4 (71.4°N, 43.9°W, 2713 m ASL), a few hundred kilometers west-southwest of Summit, suggest excess BC extending into the summer of 1889 along with increases in vanillic acid (VA), an indicator of biomass burning [McConnell *et al.*, 2007: and supplemental material, particularly their Figure S4]. Annual averages of VA from the D4 ice core show values of 203 ng/g (associated with 6.9 ng/g of BC), the largest VA since 1868 (<http://www.ncdc.noaa.gov/paleo/icecore/greenland/greenland.html>). Based on estimates from these data, the monthly averaged radiative forcing of the BC at D4 during the summer of 1889 was on the order of 0.5 W/m² [McConnell *et al.*, 2007: and Supplemental Material]. As noted by McConnell *et al.* [2007] during the preindustrial period, a summer time maximum in BC was commonly observed due to summer biomass burning. In the summer of 1889, the unusually large BC observed gives some credibility to the back-trajectory analyses that we obtained from the 20CR data, particularly for the 5 July event. This analysis leaves open the question of whether the effect of BC on the snow, combined with the other processes that we have identified, may have combined to produce the melting observed in 1889. For this reason it will be important in the future to examine the ice core record for markers of biomass burning and other fingerprints with which to identify the origin of air masses arriving over Greenland. Analyses that include an examination of water vapor isotopes, as was done for the North Greenland Eemian Drilling Project, may prove useful as suggested for deuterium excess observations (*vis-à-vis* back trajectory analyses) to determine air mass origins whether over the Arctic ice, nearby ocean, or the tropics [Steen-Larsen *et al.*, 2013].

4. Discussion

We have examined the Greenland melt episodes of 2012 as observed at Summit Station and that of 1889 as recorded in ice cores near Summit Station. These analyses have revealed a number of critical factors that likely played a role in producing these episodes. These include warm air originating over North America in areas of drought and accompanying heat waves that are subsequently transported eastward to the Atlantic and then northward to the west coast of Greenland. The combination of warm air and moisture was seen as critical factors in setting the stage for these events given the results of Bennartz *et al.* [2013] that liquid-water clouds and warm air aloft over Summit added significantly to the surface warming on 11 July 2012. The other major factor leading to these events was an antecedent distortion of the polar vortex that created an appropriate transport path for the warm air and water vapor. In 2012, a pattern of a low pressure system over Newfoundland and a high pressure ridge intersecting the southeastern coast of Greenland favored this transport of moisture. Because synoptically driven water vapor transport from the tropics and extratropics to the high latitudes often occurs in the form of "Atmospheric Rivers" that have a narrow width, their impact on land masses such as Greenland may be geographically focused. The details of transport processes over the ice sheet, which are inferred from our diagnostic analyses, are not considered in this study but could be the subject of future observation and modeling studies focusing on the west coast of Greenland. Given that the occurrence of North American heat waves, distortions of the polar vortex as indicated in the AO index, and the formation of Atmospheric Rivers in the Northwest Atlantic are highly variable phenomena (but perhaps not disconnected given the recent identification a Wave-Five synoptic pattern as a predictor of heat waves over North America by Teng *et al.* [2013]), it is not surprising that such melt events are rare. Adding to the mix in 1889 and 2012 were relatively warm ocean waters south of Greenland that had the potential (unquantified due to lack of observations) for adding moisture to the northward moving air masses and therefore influencing cloud formation over the ice sheet.

Contributing to the rarity of 2012 was the fact that the North American drought (heat wave) of 2012 was the worst since 1895, as recently reported in the literature. We have noted from the literature that previous melting of the high Greenland ice sheet occurred relatively frequently (e.g., every 100 years or so) during the Medieval Climate Anomaly, a period that also coincided with mega-droughts in North America. This leads to the suggestion that slower processes (months to seasons) such as those associated with regional heat waves over the North American continent and warmer Northwest Atlantic ocean waters tilt the odds in favor of Greenland melt episodes but still require a number of fast processes (days to weeks) to occur with the right timing and location to produce these episodes. This is particularly true for the rapidly varying aspects of the atmospheric circulation such as the AO and synoptic processes that lead to the thin filaments of water vapor that we call Atmospheric Rivers. Of interest for further investigation will be the role of "near-misses"

in the accelerated melting of the periphery of Greenland at lower elevations, the role of biomass burning as suggested by evidence in the ice cores for 1889, the response to any future changes in the frequency of droughts over North America, and the evolution of the AMO which is known for its multi-decadal variability. Clearly, future climate trends may well presage future changes in the frequency of such events.

Acknowledgments

We are indebted to the anonymous reviewers who stimulated a number of improvements to the manuscript and figures. We are also indebted to Gary Wick for providing the SSM/I Imagery, to Cathy Smith for development of Reanalysis and trajectory display tools, to Jeff Whitaker for the 20CR ensemble spread results, to Dustin Swales for access to the CFSR results, and to Don Murray for his development of visualization tools. The Ilulissat daily minimum temperature and precipitation data were provided by H.C. Steen-Larsen, obtained from the archives of the Danish Meteorological Institute. Meteorological observations for Ilulissat for 2012 were downloaded from <https://weatherspark.com>. Support for the Twentieth Century Reanalysis Project dataset is provided by the US Department of Energy, Office of Science Innovative and Novel Computational Impact on Theory and Experiment (DOE INCITE) program, and Office of Biological and Environmental Research (BER), and by the National Oceanic and Atmospheric Administration Climate Program Office. The ICECAPS field measurements at Summit are supported by the US National Science Foundation under Grants ARC-0856773, 0904152, and 0856559 as part of the Arctic Observing Network (AON) program.

References

- Alley, R., and S. Anandakrishnan (1995), Variations in melt-layer frequency in the GISP2 ice core: Implications for Holocene summer temperatures in Greenland, *Ann. Glaciol.*, *21*, 64–70.
- Arno, S. F., and S. Allison-Bunnell (2002), *Flames in Our Forest, Disaster or Renewal*, 227 pp., Island Press, Washington, D. C., ISBN 1-55963-882-6.
- Bennartz, R., M. D. Shupe, D. D. Turner, V. P. Walden, K. Steffen, C. J. Cox, M. S. Kulie, N. B. Miller, and C. Pettersen (2013), July 2012 Greenland melt extent enhanced by low-level liquid clouds, *Nature*, *496*(7443), 83–86.
- Box, J. E., L. Yang, D. H. Bromwich, and L. S. Bai (2009), Greenland ice sheet surface air temperature variability: 1840–2007, *J. Clim.*, *22*(14), 4029–4049.
- Compo, G. P., et al. (2011), The Twentieth Century Reanalysis Project, *Q. J. R. Meteorol. Soc.*, *137*(654), 1–28.
- Cook, E. R., R. Seager, R. R. Heim Jr., R. S. Vose, C. Herweijer, and C. Woodhouse (2010), Megadroughts in North America: Placing IPCC projections of hydroclimatic change in a long-term palaeoclimate context, *J. Quat. Sci.*, *25*(1), 48–61.
- Dee, D. P., et al. (2011), The ERA-Interim reanalysis: configuration and performance of the data assimilation system, *Q. J. R. Meteorol. Soc.*, *137*(656), 553–597.
- Fettweis, X., E. Hanna, C. Lang, A. Belleflamme, M. Epicum, and H. Gallee (2013), Important role of the mid-tropospheric atmospheric circulation in the recent surface melt increase over the Greenland ice sheet, *Cryosphere*, *7*(1), 241–248.
- Hanna, E., J. M. Jones, J. Cappelen, S. H. Mernild, L. Wood, K. Steffen, and P. Huybrechts (2013), The influence of North Atlantic atmospheric and oceanic forcing effects on 1900–2010 Greenland summer climate and ice melt/runoff, *Int. J. Climatol.*, *33*(4), 862–880.
- Harris, J. M., and J. D. W. Kahl (1994), Analysis of 10-day isentropic flow patterns for Barrow, Alaska - 1985–1992, *J. Geophys. Res.*, *99*(D12), 25,845–25,855, doi:10.1029/94JD02324.
- Herweijer, C., R. Seager, E. R. Cook, and J. Emile-Geay (2007), North American droughts of the last millennium from a gridded network of tree-ring data, *J. Clim.*, *20*(7), 1353–1376.
- Hoerling, M., and A. Kumar (2003), The perfect ocean for drought, *Science*, *299*(5607), 691–694.
- Hoerling, M., J. Eischeid, A. Kumar, R. Leung, A. Mariotti, K. Mo, S. Schubert, and R. Seager (2014), Causes and predictability of the 2012 great plains drought, *Bull. Am. Meteorol. Soc.*, *95*, 269–282.
- Kanagaratnam, P., S. P. Gogineni, N. Gundestrup, and L. Larsen (2001), High-resolution radar mapping of internal layers at the North Greenland Ice Core Project, *J. Geophys. Res.*, *106*(D24), 33,799–33,811, doi:10.1029/2001JD900191.
- Kepfield, S. S. (1998), "They Were in Far Too Great Want": Federal Drought Relief to the Great Plains, 1887–1895, *South Dakota History*, *28*, 244–270.
- Kingsmill, D. E., P. J. Neiman, B. J. Moore, M. Hughes, S. E. Yuter, and F. M. Ralph (2013), Kinematic and thermodynamic structures of Sierra barrier jets and overrunning atmospheric rivers during a landfalling winter storm in northern California, *Mon. Weather Rev.*, *141*(6), 2015–2036.
- Lavers, D. A., and G. Villarini (2013), The nexus between atmospheric rivers and extreme precipitation across Europe, *Geophys. Res. Lett.*, *40*, 3259–3264, doi:10.1002/grl.50636.
- Kanamitsu, M., W. Ebisuzaki, J. Woollen, S.-K. Yang, J. J. Hnilo, M. Fiorino, and G. L. Potter (2002), NCEP-DOE AMIP-II Reanalysis (R-2), *Bull. Am. Meteorol. Soc.*, *83*, 1631–1643.
- McConnell, J. R., R. Edwards, G. L. Kok, M. G. Flanner, C. S. Zender, E. S. Saltzman, J. R. Banta, D. R. Pasteris, M. M. Carter, and J. D. W. Kahl (2007), 20th-century industrial black carbon emissions altered arctic climate forcing, *Science*, *317*(5843), 1381–1384.
- Meece, D. A., A. J. Gow, P. Grootes, P. A. Mayewski, M. Ram, M. Stuiver, K. C. Taylor, E. D. Waddington, and G. A. Zielinski (1994), The accumulation record from the GISP2 core as an indicator of climate-change throughout the Holocene, *Science*, *266*(5191), 1680–1682.
- Merrill, J. T., R. Bleck, and L. Avila (1985), Modeling atmospheric transport to the Marshall Islands, *J. Geophys. Res.*, *90*(D7), 2927–2936.
- Neiman, P. J., F. M. Ralph, G. A. Wick, J. D. Lundquist, and M. D. Dettinger (2008), Meteorological characteristics and overland precipitation impacts of atmospheric rivers affecting the West Coast of North America based on eight years of SSM/I satellite observations, *J. Hydrometeorol.*, *9*(1), 22–47.
- Nghiem, S. V., D. K. Hall, T. L. Mote, M. Tedesco, M. R. Albert, K. Keegan, C. A. Shuman, N. E. DiGirolamo, and G. Neumann (2012), The extreme melt across the Greenland ice sheet in 2012, *Geophys. Res. Lett.*, *39*, doi:10.1029/2012GL053611.
- Noone, D., and I. Simmonds (1999), A three-dimensional spherical trajectory algorithm. Research Activities in Atmospheric and Oceanic Modelling, *Rep. 28, WMO/TD-No. 942*, edited by H. Ritchie, World Meteorological Organization, 3.26–3.27.
- Overland, J. E., J. A. Francis, E. Hanna, and M. Y. Wang (2012), The recent shift in early summer Arctic atmospheric circulation, *Geophys. Res. Lett.*, *39*, L19804, doi: 10.1029/2012GL053268
- Persson, P. O. G., P. J. Neiman, B. Walter, J. W. Bao, and F. M. Ralph (2005), Contributions from California coastal-zone surface fluxes to heavy coastal precipitation: A CALJET case study during the strong El Niño of 1998, *Mon. Weather Rev.*, *133*(5), 1175–1198.
- Ralph, F. M., and M. D. Dettinger (2012), Historical and National Perspectives on Extreme West Coast Precipitation Associated with Atmospheric Rivers during December 2010, *Bull. Am. Meteorol. Soc.*, *93*(6), 783–790.
- Ralph, F. M., P. J. Neiman, and G. A. Wick (2004), Satellite and CALJET aircraft observations of atmospheric rivers over the eastern north pacific ocean during the winter of 1997/98, *Mon. Weather Rev.*, *132*(7), 1721–1745.
- Ralph, F. M., P. J. Neiman, and R. Rotunno (2005), Dropsonde observations in low-level jets over the northeastern Pacific Ocean from CALJET-1998 and PACJET-2001: Mean vertical-profile and atmospheric-river characteristics, *Mon. Weather Rev.*, *133*(4), 889–910.
- Rayner, N. A., D. E. Parker, E. B. Horton, C. K. Folland, L. V. Alexander, D. P. Rowell, E. C. Kent, and A. Kaplan (2003), Global analyses of sea surface temperature, sea ice, and night marine air temperature since the late nineteenth century, *J. Geophys. Res.*, *108*(D14), 4407, doi:10.1029/2002JD002670.
- Rogers, J. C., D. J. Bathke, E. Mosley-Thompson, and S. H. Wang (2004), Atmospheric circulation and cyclone frequency variations linked to the primary modes of Greenland snow accumulation, *Geophys. Res. Lett.*, *31*, L23208, doi:10.1029/2004GL021048.
- Saha, S., et al. (2010), The NCEP Climate Forecast System Reanalysis, *Bull. Am. Meteorol. Soc.*, *91*(8), 1015–1057.

- Sand, M., T. K. Berntsen, Ø. Seland, and J. E. Kristjánsson (2013), Arctic surface temperature change to emissions of black carbon within Arctic or midlatitudes, *J. Geophys. Res. Atmos.*, *118*, 7788–7798, doi:10.1002/jgrd.50613.
- Shin, S. I., P. D. Sardeshmukh, and R. S. Webb (2010), Optimal tropical sea surface temperature forcing of North American drought, *J. Clim.*, *23*(14), 3907–3917.
- Shupe, M. D., et al. (2013), High and dry: New observations of tropospheric and cloud properties above the Greenland Ice Sheet, *Bull. Am. Meteorol. Soc.*, *94*(2), 169–186.
- Steen-Larsen, H. C., et al. (2013), Continuous monitoring of summer surface water vapor isotopic composition above the Greenland Ice Sheet, *Atmos. Chem. Phys.*, *13*(9), 4815–4828.
- Tande, G. F. (1979), Fire history and vegetation pattern of coniferous forests in Jasper National Park, Alberta, *Can. J. Botany-Revue Canadienne De Botanique*, *57*(18), 1912–1931.
- Tedesco, M., X. Fettweis, T. Mote, J. Wahr, P. Alexander, J. E. Box, and B. Wouters (2013), Evidence and analysis of 2012 Greenland records from spaceborne observations, a regional climate model and reanalysis data, *Cryosphere*, *7*(2), 615–630.
- Teng, H., G. Branstator, H. Wang, G. Meehl, and W. Washington (2013), Probability of US heat waves affected by a subseasonal planetary wave pattern, *Nat. Geosci.*, *6*, 1056–1061, doi:10.1038/ngeo1988.
- Vinther, B. M., K. K. Andersen, P. D. Jones, K. R. Briffa, and J. Cappelen (2006), Extending Greenland temperature records into the late eighteenth century, *J. Geophys. Res.*, *111*, D11105, doi:10.1029/2005JD006810.
- Whitaker, J. S., and T. M. Hamill (2002), Ensemble data assimilation without perturbed observations, *Mon. Weather Rev.*, *130*(7), 1913–1924.
- Zhu, Y., and R. E. Newell (1998), A proposed algorithm for moisture fluxes from atmospheric rivers, *Mon. Weather Rev.*, *126*(3), 725–735.